Iranian Journal of Physics Research, Vol. 21, No. 3, 2021

The effect of partial Nb doping on magnetic and electrical behavior of Y-123 superconductors with Nano CuO

R Hajilou and H Sedghi Gamchi
Superconductivity Research Center, Department of Physics, Faculty of Science, Urmia University, Urmia, Iran

E-mail: rahil.hajilou@yahoo.com

(Received 25 June 2020 ; in final form 01 February 2021)

Abstract
We have investigated the effect of Niobium and Nano CuO (40 nm) doping$Y_{1-x}Nb_xBa_2Cu_3O_{7-\delta}$ compounds with $0.00 \leq x \leq 0.05$ wt. %, prepared by the conventional solid-state method by means of XRD, SEM, R(T) and magnetic loops (M−H) measurements. The critical current densities, J_c as a function of temperature have been calculated using the critical state model from the hysteresis loops up to 1 kG at the temperature range of 10-60 K. Magnetic flux pinning, F_p of samples was calculated by using Lorentz force. The temperature dependence of the electrical resistivity measurement curves indicated that the sample with x=0.01 wt.% has a high transition temperature, T_c. XRD analysis shows a shorter c axis lattice parameter and higher orthoromthcity than the pure Y-123 and other Nb-doped samples. It was also found from J_c and F_p measurement, that the 0.01 wt.% Nb substation for the Y on YBCO superconductor improves the J_c and F_p.

Keywords: High-Tc superconductors; X-ray; Critical current density (Jc); Flux pinning (Fp)

1. Introduction

Among the four basic families of La, Y, Bi, and Tl based superconductors cuprate High-T_c crystalline structure, YBa2Cu3O7-σ (YBCO) is a High-Tc superconductor for most bulk applications with 77 K. This material also allows high critical current densities J_c in the presence of applied magnetic fields [1-3]. The effect of impurity substitutions on the transport, magnetic, and superconducting properties of High-T_c superconductors may provide clues to understanding some of the unusual normal-state and superconducting properties of these materials. The interest in doping has focused on Ag due to its good results obtained in improving the performance of YBCO [4-5]. $YBa_2Cu_3O_{7-\delta}$ is an attractive material for investigation due to their varying critical transition temperature with oxygen content and strong flux pinning capability in high magnetic fields. It is well known that the oxygen content affects the crystal structure, electron-hole transport and superconducting properties in Y_{123}. It is also realized that the superconducting transition temperature sensitively depends on both the hole concentration in the CuO_2 planes and the relative concentration of the oxygen within the planes [6-8]. It has reported that nanostructure materials and carbon−based compounds doping in High-temperature superconductors create high J_c at high magnetic fields [9,10]. At the lower magnetic field, precipitates like $Y_2BaCuNbO_x$ [11] has been found to act as pinning centers. The addition of Al_2O_3 [12] and $BaZrO_3$ [13] nanoparticles to YBCO improve pinning has attracted much scientific attention. In this paper, the samples with a stoichiometry of $Y_{1-x}Nb_xBa_2Cu_3O_{7-\sigma}$ were fabricated by a conventional solid-state reaction technique. Structural analysis of the samples was investigated by XRD and SEM measurements. The electrical properties of the samples were exanimated by R−T measurements. Magnetic properties, the critical current densities and pinning forces of the prepared samples also were calculated from the dc magnetization measurements.

2. Experimental

$Y_{1-x}Nb_xBa_2Cu_3O_{7-\delta}$ samples, with x = 0.0, 0.01, 0.02 and 0.05 substitutions were prepared from ultra-fine and high grade purity Y_2O_3, Nb_2O_5, $BaCO_3$ (purity ≥ 99.9%) and Nano copper oxide (CuO 99% APS: 40 nm) using the conventional solid-state reaction method. The starting powders in stoichiometric proportions were weighted

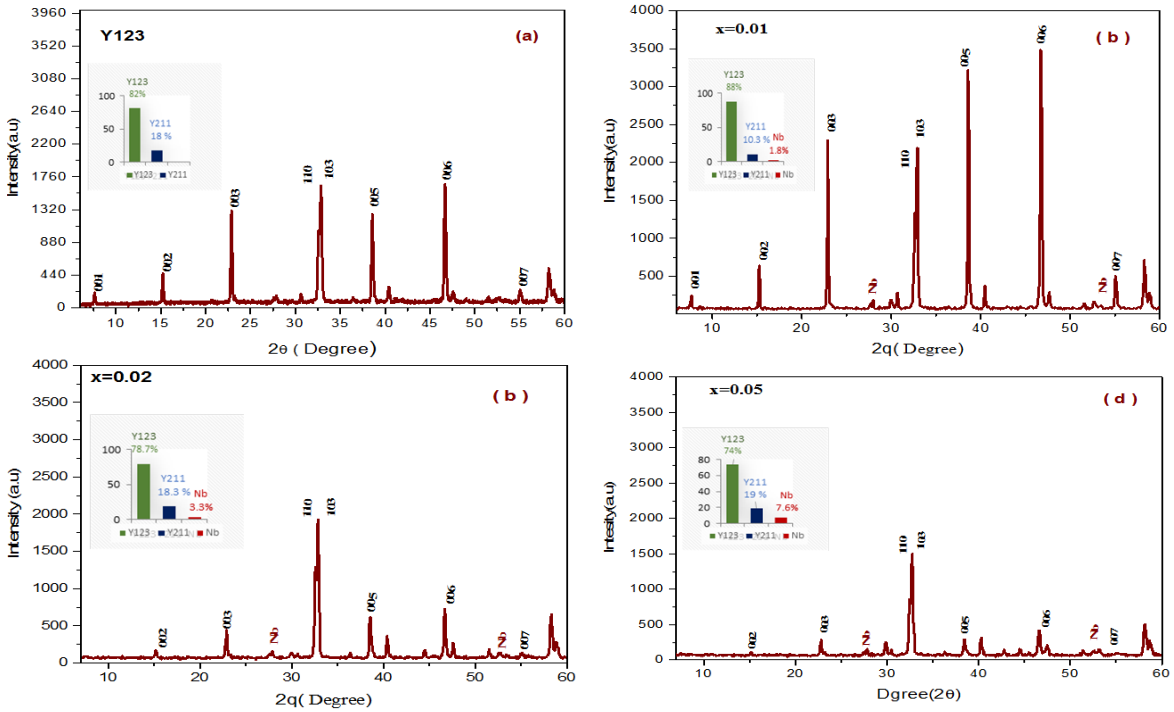

Fig 1. a-d XRD patterns of $Y_{1-x}Nb_xBa_2Cu_3O_{7-\partial}$ samples with x = 0.0, 0.01, 0.02 and 0.05 Insets demonstrate: volume fractions of Y-123, Y-211 and Nb.

and well mixed approximately for 45 min. The thoroughly mixed powders were then pelletized by pressing into a 30mm diameter steel die (carver 4387. 4SD0B00) under 50 MPa pressure. The samples in the furnace were heated to 720 ^{0}C at the rate of 120 ^{0} C/h and heated at 720 ^{0}C for 12 hours followed by heating to 930 ^{0}C at the rate of 5 ^{0}C/min and were annealed at 930^0 C for 12 h. Finally, the samples were furnace cooled to room temperature. After this first sintering process, all the samples had a gray color with same cracks. In the second cycle of the heating process, the samples were re-ground and pressed into pellets with a 30 mm diameter and an approximate thickness of 2.2 mm under 100 MPa pressure. Pellets were then placed into a furnace and heated to 930 ^{0}C at the rate of 2 ^{0}C/min. They were left to react at this temperature for 24 h. Finally, the temperature was decreased to720 ^{0}C at a rate of 2 ^{0}C/min and then furnace-cooled to room temperature in flowing oxygen with a cooling rate of 1 ^{0}C/min. The low cooling rate in flowing oxygen was used in order to improve oxygen uptake in the samples. At the last sintering process, all the samples had a black color. Unlike the first processing cycle, the products of the second cycle were uniform and almost without any cracks. X-ray diffraction measurements were made in the range of $6^\circ \leq 2\theta \leq 60^\circ$ with CuK_α radiation source ($\lambda = 1.5406$ Å). X-pert High Score software was used to determine the lattice parameters, peak positions and peak intensities. The grain morphology of the surface of the samples was analyzed by scanning electron microscopy (SEM). For measurement of the dc resistivity of samples as a function of temperature, the standard four-point probe method with silverpoint contacts was used. The transition temperature T_c was determined as a function of temperature at zero resistivity. Isothermal hysteretic loops M-H curves was performed using cryogenic design physical properties measurement system (ppms) model 3045, upto 70kG using the so-called vsm option. The critical current density, J_c was calculated using the Bean model for the pure and Nb substituted x=0.01 samples at 10-60K up to 60kG applied magnetic field. The pinning force, F_p depending on applied magnetic field and temperature was calculated from isothermal M–H measurement.

3. Results and Discussion

3. 1. XRD results

Figure 1 shows the XRD patterns of the samples a to d, which Nb was substituted in the form of Nb_2O_5. Obtained results from XRD patterns indicated that the peaks of the pure (YBCO) and Nb-doped $Y_{1-x}Nb_xBa_2Cu_3O_{7-\sigma}$ samples were well matched to the orthorhombic Y123 structure. It can be seen from the XRD patterns of the pure Y_{123} and the alloyed samples that all the high-intensity peaks in the XRD patterns are assigned to $Y_1Ba_2Cu_3O_{7-\partial}$ phase indicating that Nb doping atoms have not been effected the orthorhombicity of YBCO compound. There are also a few low-intensity peaks assigned to the unheated materials and green insulating phase, Y211 which is commonly one of the impurities between the Y123 grains. It has been argued that particles around the grains may act as a catalyst to improve the structural quality at grain boundaries observed by other research groups [14]. The oxygen contents of the samples were calculated using Wolf's formula [15]:

$$7 - \delta = 76.4 - 5.95\ c \quad (Å) \qquad (1)$$

Table 1. Characteristic temperatures, lattice parameters, hole –carrier concentration per Cu ion and orthorombicity parameters for all the $Y_{1-x}Nb_xBa_2Cu_3O_{7-\delta}$ samples.

Nb content x (wt%)	Tc, onset (K)	$Tc,0$ (K)	ΔT_c (K)	a (Å)	b (Å)	c (Å)	Δ=(b-a)/(b+a)	O-content	P
0.0	90.5	85	5.5	3.82	3.88	11.68	0.007792	6.90	0.1908
0.01	91.5	87.9	3.6	3.803	3.886	11.669	0.009973	6.97	0.1902
0.02	84.7	80.5	4.2	3.816	3.878	11.68	0.008512	6.90	0.1925
0.05	81.9	77.4	4.5	3.8263	3.8813	11.707	0.007136	6.74	0.1919

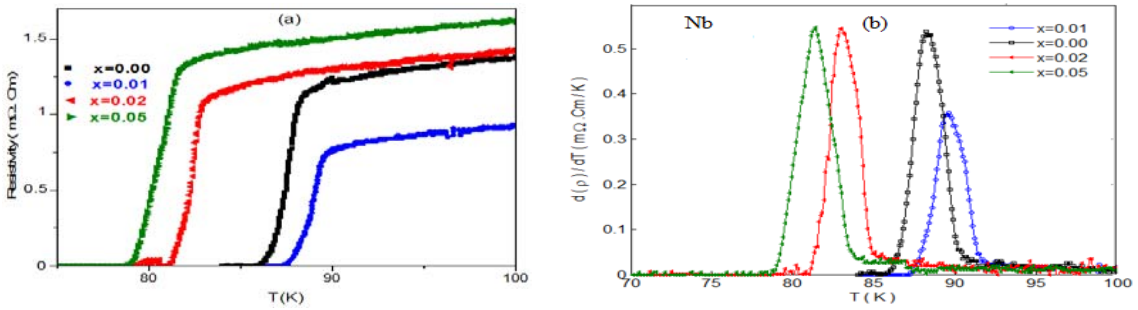

Fig 3. a and b **ρ**–T curves and its temperature derivative of the$Y_{1-x}Nb_xBa_2Cu_3O_{7-\delta}$ with x = 0, 0.01, 0.02 and 0.05.

Where (7-δ) is the oxygen content of the sample and 'c' is axis lattice parameter. It is well established that both the 'a' and 'b' lattice parameters in the YBCO system have a nonlinear relation in the orthorhombic phase, while the c-axis lattice parameter and unit-cell volume, show a linear general behavior as a function of oxygen content. The higher the oxygen content of sample the lower the c-axis lattice parameter [16]. The calculated unit cell parameters of the pure and the Nb-doped samples, orthorhombic strains, Δ = (b-a) / (b+a), hole-carrier concentration per Cu ion and transition temperature of the samples are presented in Table 1. A brief look at the table shows that despite slight variations in the lattice parameters 'a', 'b' and 'c', the unit cell parameters of the alloy samples are very close to that of the Y123 sample and a slight decrease in the c-axis length shows a slight increase in the oxygen content in the sample with x=0.01. The decrease in c axis parameter is probably related to the difference in (007) reflection in XRD patterns of this sample. The difference on the unit cell parameters can be due to occupation of the Nb ions to interstitial sites [17].

We also have calculated the hole-carrier concentration per Cu ion, P for our studied samples using a parabolic formula which is generic to the whole class of high T_c superconductors as follows [18-19].

$$\left[\frac{Tc(x)}{Tc(0)}\right] = 1 - 82.6\,(P - 0.16)^2 \qquad (2)$$

Where T_c (0) and T_c(x) are the critical temperatures for the pure and doped samples, respectively. P is the hole-carrier concentration per Cu ion. The relative volume fractions of Y-123, Y-211 and Nb phases are estimated by comparing the intensities of the whole pattern [20], according to the relations:

$$[Y-123]\% = \frac{\sum I[Y123]}{\sum I[Y123] + \sum I[Y211]} \qquad (3)$$

$$[Y-211]\% = \frac{\sum I[Y211]}{\sum I[Y123] + \sum I[Y211] + \sum I[Nb]} \qquad (4)$$

$$[Nb]\% = \frac{\sum I[Nb]}{\sum I[Y123] + \sum I[Y211] + \sum I[Nb]} \qquad (5)$$

Where 'I' is the peak intensity of the present phases above the baseline. volume fractions of Y-123, Y-211 and Nb phases for all our samples are illustrated by comparing the intensities of the whole pattern in the insets of the XRD patterns. It can be seen from the XRD patterns, that the volume fraction of Y-123 phase has been increased in the Nb-doped x = 0.01 wt.% sample.

3. 2. Electrical resistivity

We measured the electrical resistivity versus temperature (ρ-T) through the four-probe method. The variation of the electrical resistivity as a function of temperature along with its temperature derivative for the $Y_{1-x}Nb_xBa_2Cu_3O_{7-\delta}$ samples. It is clear from these figures that all the samples possessed metallic behavior above T_c^{onset} and go to superconducting state at T_c^{offset} are shown in Fig. 3a and b. The transition width, ΔT for the Sm-doped samples show a broadened resistive transition to the fully superconducting state, showing the increase in the weak link between superconducting grains. It may be seen from (ρ-T) figures that the sample with Nb-doped x = 0.01 wt.% in the Y_{123} system has a higher transition temperature than the other samples.

3. 3. Magnetic properties

Since the sample with Nb-doped x = 0.01 wt.% in the Y_{123} system shows critical temperature higher than the other samples even the pure Y-123, so we concentrated the magnetic measurements on the positive effect of partially Nb-doped sample and cuprated the results with the pure Y-123 sample. Isothermal magnetic hysteresis loops (M-H) curves for the pure Y_{123} and x = 0.01 at different constant temperatures of 10, 20, 30, 40, 50 and

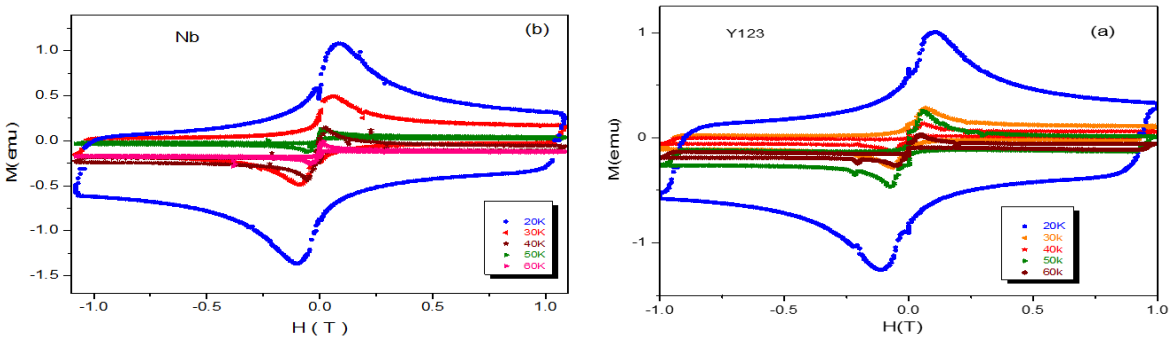

Fig. 4 Displays the isothermal magnetization versus filed curves (M-H loop) at 20 K, 30 K,40 K, 50 K and 60 K for the a the pure Y_{123} and b the Nb x = 0.01 samples.

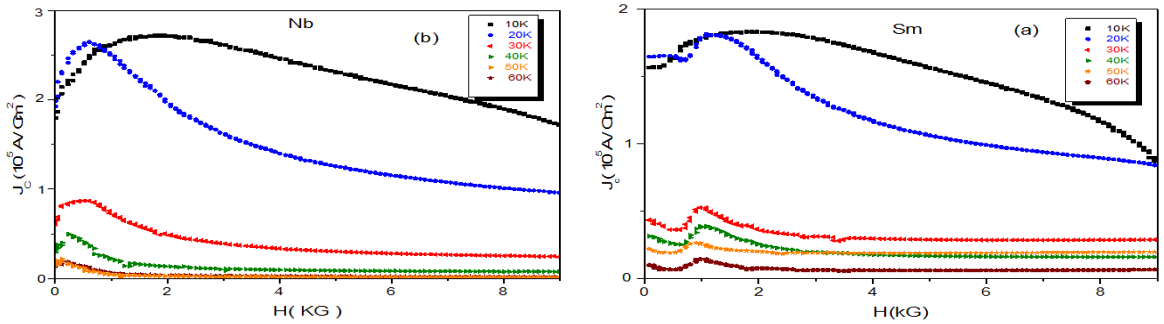

Fig. 5 The plot of J_c as a function of magnetic field for a the pure Y_{123} and b the Nb- doped x = 0.01 samples.

60 K up to of 10 kG are shown in Fig. 4a and b. The higher the pinning strength, the bigger the critical current, hence the wider the hysteresis loops. It is well known that the width and behavior of hysteresis loops are related to the characteristics of the bulk J_c in HTSC' s and its dependence on the magnetic flux density [21]. By using Bean's critical state model, J_c of the samples was calculated from the hysteresis loops [22]. In the Bean's critical state model, the J_c is proportional to the width of the hysteresis loops $\Delta M = |M^+ - M^-|$ calculates from formula given by:

$$J_c = 20\frac{\Delta M}{a(1-a/3b)} \quad (6)$$

where J_c is the critical current density in amperes per square centimeter of a sample and M^+ and M^- magnetizations are obtained from the intersections of M-H loops increasing and decreasing of measuring magnetic field respectively. ΔM is measured in electromagnetic units per cubic centimeter, a and b (a < b) are the sample dimensions perpendicular to the applied field. The applied magnetic field dependence of J_c(H), at 10, 20, 30, 40, 50 and 60 K for the samples with x = 0.0 and 0.01 are presented in Fig. 5. The Nb-doped x = 0.01 sample and pure Y_{123} at 10 K for the applied magnetic field of 1 kG show J_c values $J_c^{max} = 2.73 \times 10^5$ A/cm^2 and 1.8×10^5 A/cm^2 respectively, the Nb-doped x = 0.01 sample shows J_c^{max} = approximately 1.52 times bigger than the pure Y-123 sample. The J_c values in the applied magnetic field decrease with increasing measuring constant temperature as shown in Fig.5a and b. There is an electromagnetic interaction force between the flox lines and the current density below Tc through the Lorentz force, F_L [23] as:

$$F_L = J_c \times B \quad (7)$$

where J_c is the current density and B is the flux density in the sample. Fluxoids remain stationary and the superconducting behavior of the material maintains with zero resistance as long as the pinning force, F_p, equals at least to F_L. When F_L acting the fluxoids exceeds F_p, the fluxoids begin to move across the sample and the material becomes resistive. Comparison of Fig. 6a for pure Y_{123} and b for the Nb-doped sample shows that measured F_p for the Nb-doped x = 0.01 sample is significantly higher than that of the pure Y_{123}. The Nb-doped x = 0.01 sample and pure Y123 at 10 K for the applied magnetic field of 9 kG how F_p values $F_p^{max} = 1.55 \times 10^6$ N/cm^3 and $F_p^{max} = 0.96 \times 10^6$ N/cm^3 respectively. The measured value of F_p at 50 K in 15 wt.% Ag doped YBCO system has been reported to be 3.7×10^5 N/cm^3 [24]. Thus the addition of 0.01 wt.% Nb enhances J_c by a factor of 3 with respect to Ag added samples. The enhancement of J_c in Nb-doped x = 0.01 sample is also more than that reported by the other out hers [25-26].

4. Conclusion

We have studied the effect of Nb substituted $Y_{1-x}Nb_xBa_2Cu_3O_{7-\partial}$ composites on the structural, electrical, and magnetic properties of High-temperature YBCO superconductor. Through XRD and SEM analysis, we found that all the measured samples had orthorhombic structure. Based on our XRD, SEM and magnetization measurements, we deduce that the optimal addition of

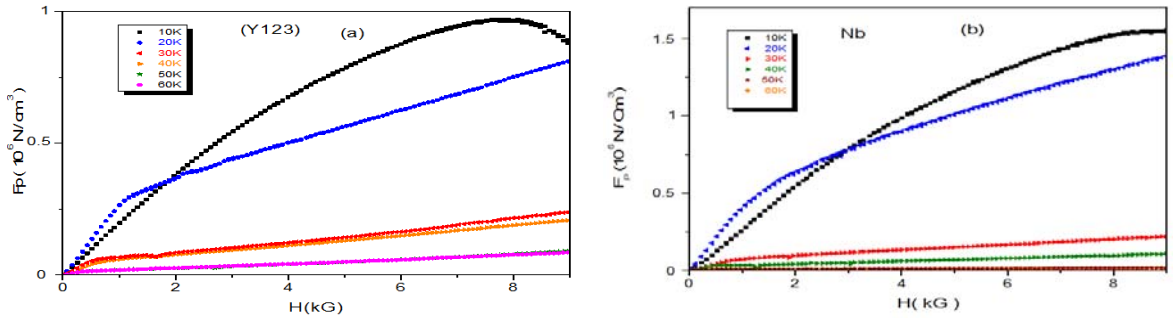

Fig 6. F_P-H dependences at 10 K, 20 K, 30 K, 40 K, 50 K and 60 K a for the pure Y_{123} and b Nb- doped x = 0.01 samples.

the Nb-doped x = 0.01 sample has a significant enhancement in the Superconductivity parameters. Both F_p and J_c have been found to increase in the Nb-doped x = 0.01 sample over the whole range of the applied magnetic fields. In the Nb-doped x = 0.01 sample it has been observed a 1.52-folder increase in Jc at 10 K with respect to the pure sample.

References

1. S Sathyamurthy, A Parikh, and K Salama, *Processing of polycrystalline HTCS, for high current transport applications, Physica* C **271** (1996) 349. https://doi.org/10.1016/S0921-4534(96)00553-9.
2. M Murakami, *electromagnetic applications of melt-processed YBCO, Ceramics Int.* **23** (1997) 203. https://doi.org/10.1016/S0272-8842(96)00026-0.
3. K Nakazatoa, M Muralidhara, M R Koblischkaab, and M Murakamia, *Fabrication of bulk Y–Ba–Cu–O superconductors with high critical current densities through the infiltration-growth process, Solid State Commun* **63** (2014) 129. https://doi.org/10.1016/j.cryogenics.2014.04.003.
4. M Tepe, I Avci, H Kocoglu, and D Abukay, *Investigation of the variation in weak-link profile of* $YBa_2Cu_{3-x}Ag_xO_{7-\delta}$ *superconductors by Ag doping concentration, Solid State Commun* **131** (2004) 319. https://doi.org/10.1016/j.ssc.2004.05.015.
5. A Yıldız, K Kocabaş, and G Akyüz, *Dependence of the Structural, Electrical and Magnetic Properties of YBa2Cu3O7−δ Bulk Superconductor on the Ag Doping J Supercond and Nov Magn*. **25** (2012) 1459. https://doi.org/10.1007/s10948-012-1482-8.
6. R J Cava, B Batlogg, C H Chen, E A Reitman, S M Zahurak and D werder, *Single-phase 60-K bulk superconductor in annealed YBa2Cu3O7−δ (0.3<δ<0.4) with correlated oxygen vacancies in the Cu-O chains, Phys. Rev*. B **36** (1987) 5714. https://doi.org/10.1103/PhysRevB.36.5719.
7. L Jansen, R B lock, *Effect of iodine intercalation on superconductivity in the high-*T_C *series* $Bi_2Sr_2Ca_{N-1}Cu_NO_{2N+4+\delta}$, *N=1–3, and in the yttrium doped N=2 compound. A quantitative analysis on the basis of indirect exchange pairing, Phys*. A **277** (2000) 183. https://doi.org/10.1016/0378-4371(93)90240-5.
8. S Nakajima, M Kikachi, Y Syono, T OKO, D Shindo, K Hiraga, N Kobayashi, H Iwasaki, Y Muto, *Synthesis of bulk high* T_c *superconductors of* $TlBa_2Ca_{n-1}Cu_nO_{2n+3}$ *(n = 2 − 5), Physica,* C **158** (1989) 471. https://doi.org/10.1016/0921.4534(89)90246-3.
9. S Dadras and M Ghavamipour, *Investigation of the properties of carbon-base nanostructures doped* $YBa_2Cu_3O_{7-\delta}$ *high temperature superconductor, Physica* B **484** (2016) 13-17. https://doi.org/10.1016/j.physb.2015.12.025.
10. S Dadras, Y Liu, Y S Chai, V Daadmehr, K H Kim, *Increase of critical current density with doping carbon nano-tubes in* $YBa_2Cu_3O_{7-\delta}$, *Physica* C **469** (2009) 55. https://doi.org/10.1016/j.physc.2008.11.004.
11. M N Hasan, M Kiuchi, E S Otabe, T Matsuhita, M Muralidhar, *Flux pinning properties of (Nd, Eu, Gd)* $Ba_2Cu_3O_y$ *(NEG-123) superconductor with 211 phase particles Supercond, Sci. Technol* **20** (2007) 345. https://doi.org/10.1088/0953-2048/20/4/008.
12. A Mellekh, M Zouaoui, F B Azzouz, M Annabi, and M B Salem, *Nano-* Al_2O_3 *particle addition effects on Y* $Ba_2Cu_3O_y$ *superconducting properties Solid State Commun*. **140** (2016) 318. https://doi.org/10.1016/j.ssc.2006.08.008.
13. C Xu, A. Hu, M Ichihara, N Sakai, I Hirabayashi, and M Izumi, *Physica C, Enhanced flux pinning of air-processed Gd123 by doping* ZrO_2 *nanoparticles* **460** (2007) 1341. https://doi.org/10.1016/j.physc.2007.04.168**.**
14. A K Jha and N Khare, *Strongly, enhanced pinning force density in YBCO–*$BaTiO_3$ *nanocomposite superconductor, Physica* C **469** (2009) 810. https://doi.org/10.1016/j.physc.2009.05.008.
15. T Wolf, I Apfelstedt, W Goldcker, H Küpfer, and R Flükiger, *Preparation and characterization of isotropic and textured* $YBa_2Cu_3O_{7-x}$ *with high density and low residual resistivity, Physica* C **351** (1988) 153. https://doi.org/10.1016/0921-4534(88)90628-4.
16. R M Hazen, L W Finger, R J Angel, C T Perwitt, N L Ross, H K Mao, C G Hadidiacos, P H Hor, R L. Meng, and C W Chu, *Crystallographic description of phases in the Y-Ba-Cu-O superconductor, Phys. Rev*. **335** (1987) 7238. https://doi.org/10.1103/PhysRevB.35.7238.

17. M B Turkoz, S Nezir, C Terzioglu, A Varilci, and G Yildirim, *Investigation of Lu effect on $YBa_2Cu_3O_{7-\sigma}$ superconducting, compounds J Mater Sci. Mater Electron* **24** (2013) 896. https://doi.org/10.1007/s10854-012-0846-y.
18. M R Presland, J L Tallon, R G Buckley, R S Liu, and N E Flower, *General trends in oxygen stoichiometry effects on T_c in Bi and Tl superconductors, Physica* C **176** (1991) 95. https://doi.org/10.1016/0921-4534(91)90700-9.
19. S D Obertelli, J R Cooper, and J L Tallon, *Systematics in the thermoelectric power of High-Tc oxides, Phys. Rev.* B **46** (22) (1992) 14928. https://doi.org/10.1103/PhysRevB.46.14928.
20. J C Chen, Y Xu, M K Wu, and W Guan.: *Ion-Size Effect on Normal-State Transport Properties in $R_{0.8}Pr_{0.2}Ba_2Cu_3O_{7-y}$ Systems (R = Yb, Er, Dy, Gd, Eu, and Nd). Physical Review* B, **53** (1996) 5839. http://dx.doi.org/10.1103/PhysRevB.53.5839.
21. A Öztürka, İ Düzgünb, S çlebi.: *The effect of partial Lu doping on magnetic behaviour of YBCO (123) superconductors, J. Alloys and compound.* **495** (2010) 104. https://doi.org/10.1016/j.jallcom.2010.01.095.
22. C P Bean, *Magnetization of Hard Superconductors*, *Phys. Rev. let.* **8**, (1962) 250. https://doi.org/10.1103/PhysRevLett.8.250.
23. W C Chan, C H Chiang, and Y J Hsu, *Direct Lorentz force measurement for $YBa_2Cu_3O_{7-\delta}$ superconductor, Cryogenics* **50** (2010) 292. https://doi.org/10.1016/j.cryogenics.2010.01.002.
24. B A Malik, M A Malik, and K Asokan, *Enhancement of the critical current density in YBCO/Ag composites, Chinese Journal of the physics* **55** (2017) 170. https://doi.org/10.1016/j.cjph.2016.10.015.
25. H Huhtinen, V P S Awana, A Gupta, H Kishan, R Laiho and A V Narlikar: *Pinning centres and enhancement of critical current density in YBCO doped with Pr, Ca and Ni, Supercond. Sci. Technol*. **20** (2007) 159. https://doi:10.1088/0953-2048/20/9/S08.
26. B A Malik, M A Malik, and K Asokan, *Magneto transport study of YBCO: Ag composites, Current Applied Physics* **16** (2016) 1270 -1276. https://doi.org/10.1016/j.cap.2016.07.004.